C Reference Controller

In this appendix the design of a reference controller for the wind turbine is described. The controller is supposed to approximate the configuration of an existing control system, and is designed based on classical principles. Note that the structure of the reference controller is specified in cooperation with kk-electronic a/s and that this appendix is based on [Esbensen *et al.*, 2008, pp. 45-59].

As stated in Section 2.2 the nominal operating trajectory of the wind turbine is created to satisfy different demands below and above a certain wind speed. Since the classical control approach deals only with SISO transfer functions, and because several references exist, the control task is split into the design of multiple separate controllers.

For an overview of the structure of the classical controller refer to Figure 2.4 on Page 8. The design of the classical controller is divided into four main design steps, corresponding to the names of the sections in this appendix. These are listed below to provide an overview.

- **Controller Operating in Partial Load Operation:** Describe the design and verification of the generator torque controller. This controller operates in the partial load region and should maximize the energy production while minimizing mechanical stress and actuator usage.
- **Controller Operating in Full Load Operation:** Describe the design and verification of the speed controller and power controller. These controllers operate in the full load region and should track the rated generator speed and limiting the output power.
- **Drive Train Stress Damper:** Describe the design and verification of the drive train stress damper. The purpose of the drive train stress damper is to dampen drive train oscillations.
- **Bumpless Transfer:** Describe the design and verification of the mechanism which eliminates bumps on the control signals, when switching between the controllers in the partial load and full load regions.

Notice that the transfer functions derived throughout this appendix have been discretized to allow implementation of the controllers and filters.

C.1 Controller Operating in Partial Load Operation

At low wind speeds, i.e. in partial load operation, variable-speed control is implemented to track the optimum point on the C_p-surface for maximizing power output. The speed of the generator is controlled by regulating the torque on the generator through the generator torque controller. The purpose of this section is to go through the design of the generator torque controller. Finally, it is evaluated by simulation.

In partial load operation it is chosen to operate the wind turbine at $\beta = 0°$ since the maximum power coefficient is obtained at this pitch angle. This means that the highest efficiency is achieved for:

$$\lambda_\mathrm{opt} = \frac{\omega_\mathrm{r,opt}(t)R}{v_\mathrm{r}(t)} \quad [\cdot] \tag{C.1}$$

where:

R	is the rotor radius [m]
$v_\mathrm{r}(t)$	is the rotor effective wind speed [m/s]
λ_opt	is the tip-speed ratio maximizing the C_p-value for $\beta = 0°$ [$\cdot$]
$\omega_\mathrm{r,opt}(t)$	is the optimum rotor speed [rad/s]

In order to obtain the optimal tip-speed ratio a method is used, which suggests applying a certain generator torque as a function of the generator speed. This is described in [Johnson *et al.*, 2006, p. 74] and is referred to as the standard control law for operating variable-speed turbines. The benefit of this approach is that only the measurement of the rotor speed or generator speed is

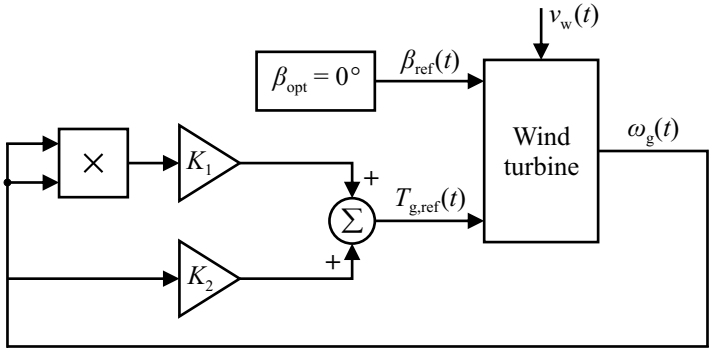

Figure C.1: *Generator torque controller for operation in the partial load region, i.e. below the rated wind speed.*

required. When utilizing this approach, the controller structure for partial load operation becomes as illustrated in Figure C.1, which will become apparent from the following text.

The principle of the standard control law is to isolate the wind speed in the definition of the tip-speed ratio, Eq. (3.7) on Page 14, and insert it into the expression for the aerodynamic torque, Eq. (3.9) on Page 15. Hence, an equation can be obtained expressing the required generator torque based on the maximum power coefficient and the optimal tip-speed ratio. The equation is now going to be derived. First, the wind speed is isolated:

$$v_r(t) = \frac{\omega_r(t)R}{\lambda(t)} \quad [\text{m/s}] \tag{C.2}$$

Secondly, this expression is inserted into Eq. (3.9) describing the aerodynamic torque:

$$\begin{aligned} T_a(t) &= \frac{1}{2\omega_r(t)}\rho A v_r^3(t) C_p\left(\lambda(t), \beta(t)\right) \\ T_a(t) &= \frac{1}{2}\rho A \frac{R^3}{\lambda^3(t)} C_p\left(\lambda(t), \beta(t)\right) \omega_r^2(t) \quad [\text{Nm}] \end{aligned} \tag{C.3}$$

Since the wind turbine includes a transmission system, the gear ratio and friction components of the drive train have to be considered when determining the generator torque corresponding to a certain aerodynamic torque. This is however not included in [Johnson *et al.*, 2006, p. 74], and in order to describe the generator torque only as function of the generator speed, the system has to be assumed in steady-state, where $\dot{\omega}_r(t) = 0$ rad/s^2, $\dot{\omega}_g(t) = 0$ rad/s^2, and $\omega_g(t) = N_g\omega_r(t)$. By doing so, Eq. (Eq. (3.19)) and Eq. (3.20) on Page 17 can be rewritten into:

$$\begin{aligned} 0 &= T_a(t) - K_{dt}\theta_\Delta(t) - B_r\omega_r(t) \quad [\text{Nm}] \\ 0 &= \frac{K_{dt}}{N_g}\theta_\Delta(t) - B_g\omega_g(t) - T_g(t) \quad [\text{Nm}] \end{aligned} \tag{C.4}$$

These equations can be combined into:

$$T_a(t) = N_g T_g(t) + \left(\frac{B_r}{N_g} + N_g B_g\right)\omega_g(t) \quad [\text{Nm}] \tag{C.5}$$

Inserting Eq. (C.5) into Eq. (C.3) in an optimal point for the power coefficient leads to the control law dictated by Eq. (C.6). Notice that the equation is based on a steady-state consideration so that actuator dynamics can also be disregarded by setting $T_{g,ref}(t) = T_g(t)$.

$$T_{g,ref}(t) = \underbrace{\frac{1}{2}\rho A \frac{R^3}{N_g^3\lambda_{opt}^3} C_{p,max}}_{K_1}\omega_g^2(t) - \underbrace{\left(\frac{B_r}{N_g^2} + B_g\right)}_{K_2}\omega_g(t) \quad [\text{Nm}] \tag{C.6}$$

where:
K_1 is the gain of the standard control law [Nm/(rad/s)^2]
K_2 is a gain compensating for frictions in the drive train [Nm/(rad/s)]

Evaluation of Controller Operating at Partial Load

Figure C.2 shows how the generator torque controller performs. It should be noted from the figure that in the first part of the simulation the output power becomes larger than the theoretically $P_{\mathrm{g,max}}(t)$, because kinetic energy from the rotor shaft is converted into electrical energy produced by the generator. Similar, $P_{\mathrm{g,max}}(t)$ is above the produced power towards the end of the time series, since the inertia of the rotor has to be accelerated before $P_{\mathrm{g,max}}(t)$ can be matched. This phenomenon is caused by ignoring dynamics in the calculation of the theoretical maximum power output.

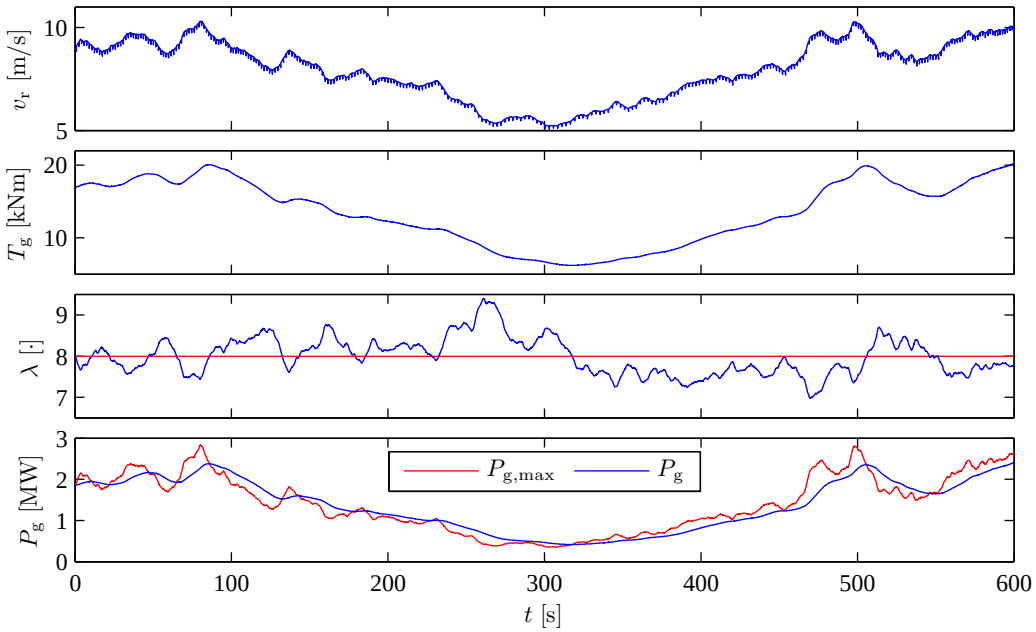

Figure C.2: *Simulation of the generator torque controller operating below rated wind speed. The lower subplot compares the power produced by the generator to the theoretical maximum power output of the wind turbine given the instant wind speed.*

The obvious disadvantage of the standard control law is that the optimum point of the C_{p}-surface must me known precisely. Even if it is assumed that this information is correct, whenever the turbine is installed, power optimization still degrades over time as a result of a changing power coefficient. According to kk-electronic a/s, the maximum power coefficient of the wind turbine blades reduces in amplitude while the relationship between tip-speed ratio, pitch angle, and C_{p}-value also changes over time, e.g. due to debris building up on the blades.

In the next section a description of the controller design for the operation at full load is provided.

C.2 Controller Operating in Full Load Operation

For the high wind speeds, i.e. in full load operation, the desired operation of the wind turbine is to keep the rotor speed and the generated power at constant values, as described in Section 2.2. The main idea is to use the pitch system to control the efficiency of the aerodynamics while applying the rated generator torque. However, in order to improve tracking of the power reference and cancel steady-state errors on the output power, a power controller is also introduced. Therefore, the purpose of this section is to go through the design of the speed controller and the power controller.

The structure of the controllers operating above the rated wind speed is shown in Figure C.3.

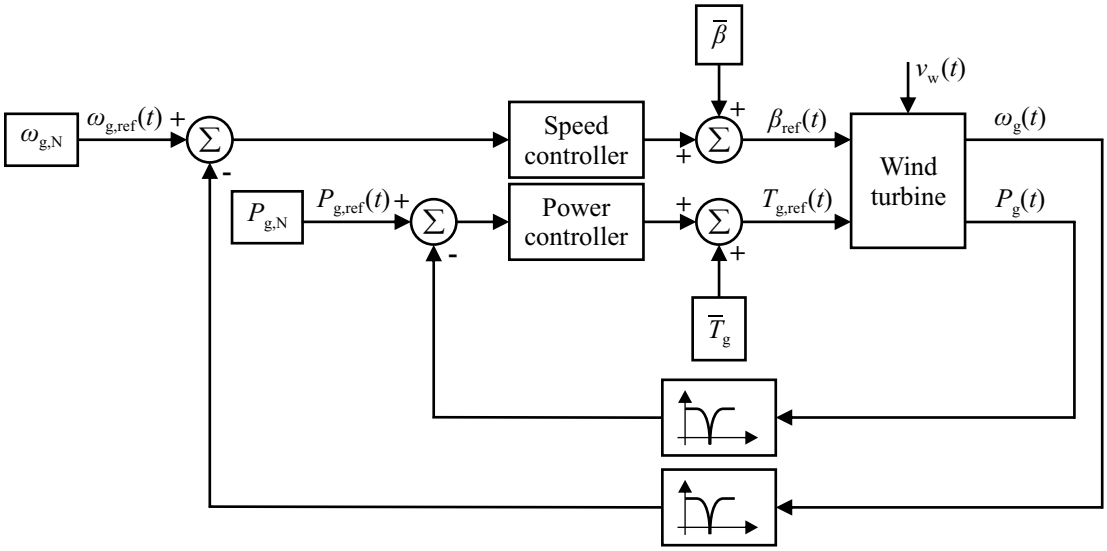

Figure C.3: *Speed controller and power controller for operation in the full load region, i.e. above the rated wind speed.*

The wind speed is considered the disturbance input to the system. However, higher frequency components such as the resonant frequency of the drive train are also apparent on the measured generator speed. Therefore, the measured generator speed is band-stop filtered before it is fed to the controller, to remove the drive train eigenfrequency from the measurement. This solution is also found in other wind turbine control schemes to mitigate the effects of drive train oscillations. The applied notch filter appears from Eq. (C.7) [East and Lantz, 2005, p. 3]. Notice that for implementation the filter is discretized using zero-order hold.

$$H_n(s) = \frac{s^2 + 2\frac{d}{c}\omega_0 s + \omega_0^2}{s^2 + 2\frac{1}{c}\omega_0 s + \omega_0^2} \quad [\cdot] \tag{C.7}$$

where:

c and d are filter coefficients; $c = 0.1$ and $d = 5$ $[\cdot]$
$H_n(s)$ is the notch filter $[\cdot]$
ω_0 is the notch frequency of the filter, which must be close to the resonant frequency to be damped [rad/s]

In the following subsection the design of the speed controller is described and evaluated. Afterwards, in the succeeding subsection, the power controller is presented.

Speed Controller

The speed controller is implemented as a PI controller that is able to track the speed reference and cancel possible steady-state errors on the generator speed. The speed controller is on the form:

$$D_s(s) = K_{ps}\left(1 + \frac{1}{T_{is} \cdot s}\right) \quad [^\circ/(\text{rad/s})] \tag{C.8}$$

where:

$D_s(s)$ is the PI controller to ensure that the generator speed follows the speed reference $[^\circ/(\text{rad/s})]$
K_{ps} is the proportional gain of $D_s(s)$ $[^\circ/(\text{rad/s})]$
T_{is} is the reset rate of $D_s(s)$ [s]

Figure C.4 shows how the partial derivative of $T_a(t)$ with respect to β varies along the nominal operating trajectory. As a consequence, a gain scheduling scheme is applied to the speed controller, dividing the full load region into two control regions.

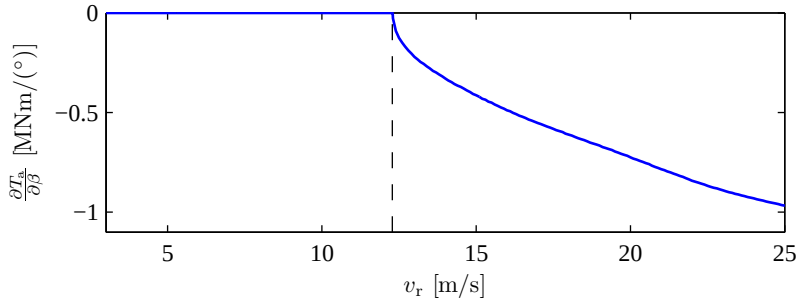

Figure C.4: *Partial derivative of $T_a(t)$ with respect to β along the nominal operating trajectory. The vertical dashed line represents the rated wind speed.*

According to Figure C.4 pitching the blades will have a larger influence on the aerodynamic torque at higher wind speeds. For this reason the gain of the speed controller should be large near the rated wind speed but smaller at higher wind speeds, which is also shown in [Hammerum, 2006, p. 30].

The optimal gain of the speed controller associated with a certain wind speed can make the system become unstable at higher wind speeds due to the increasing gain of the system. Therefore, the speed controller is configured with one set of parameters in the region corresponding to stationary wind speeds in the interval 12-15 m/s, while a smaller gain is utilized for the region covering wind speeds of 15-25 m/s. Although the system has different gains in these two region, it is possible to design the controllers so that similar transient responses of the closed-loop system are obtained.

The design procedure of finding appropriate parameters for the speed controller is initiated by determining the reset rate based on a root locus of the transfer function $H_n(s) \cdot D_s(s) \cdot \omega_g(s)/\beta_{ref}(s)$, which is the transfer function arising by opening the loop prior to the speed controller. Figure C.5 sketches an excerpt from the pole-zero map. The pole in zero originates from the integral action of the PI controller, $\omega_{pole,1}$ denotes a pole of $\omega_g(s)/\beta_{ref}(s)$, and the zero is determined by the reset rate of the speed controller. The value of $\omega_{pole,1}$ changes according to the operating point, and to obtain similar responses in the two cases, the zero in both cases are placed just to the right of $\omega_{pole,1}$. This is done to let the loci stay on the real axis. For the relevant case, the following has been utilized:

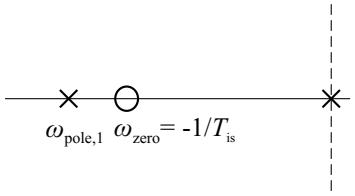

Figure C.5: *Excerpts from the root locus of the transfer function $H_n(s) \cdot D_s(s) \cdot \omega_g(s)/\beta_{ref}(s)$.*

$$T_{is} > \frac{1}{\omega_{pole,1}}$$
$$T_{is} = 1.065\frac{1}{\omega_{pole,1}} \quad [s] \tag{C.9}$$

Having determined the reset rates of the speed controllers, the proportional gains are selected in order to provide phase margins of 50°. This is verified in Figure C.6.

The parameters for the speed controllers are written in Table C.1.

Speed Controller 1		**Speed Controller 2**	
$K_{ps,1}$	$T_{is,1}$	$K_{ps,2}$	$T_{is,2}$
-6.89°/(rad/s)	25 s	-2.95°/(rad/s)	6.02 s

Table C.1: *Parameters of the speed controllers. Speed Controller 1 are designed to operate at wind speeds in the region $12-15$ m/s, while Speed Controller 2 are designed to operate at wind speeds in the region $15-25$ m/s.*

In order to evaluate the designed controllers in the extremity of their regions, the minimum and maximum parameters of the linearized model are applied. Hence, the step responses in Figure C.7

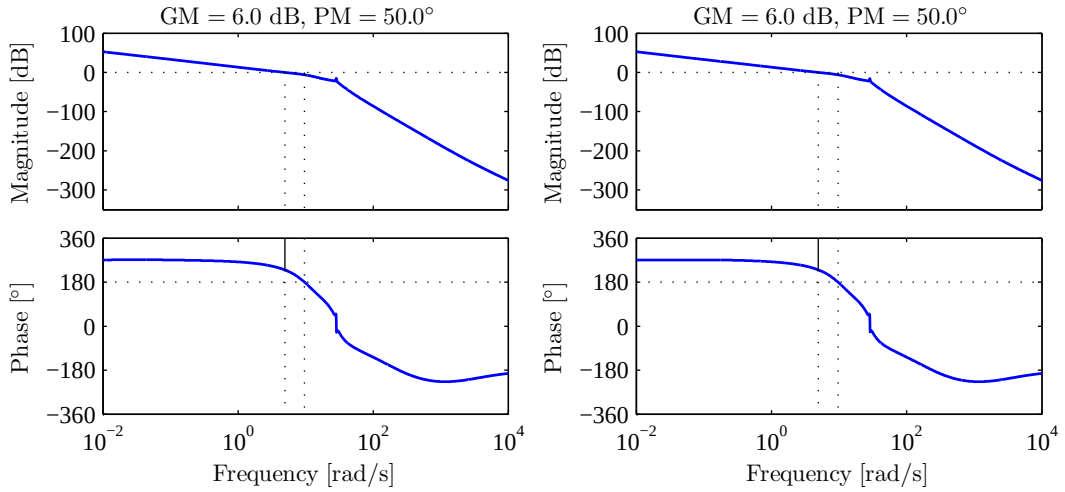

Figure C.6: *Bode plots of* $H_{\mathrm{n}}(s) \cdot D_{\mathrm{s}}(s) \cdot \omega_{\mathrm{g}}(s)/\beta_{\mathrm{ref}}(s)$. *The results in the left subplots are for Speed Controller* 1 *at an operating point wind speed of* 15 m/s, *while the right subplots display results for Speed Controller* 2 *at an operating point wind speed of* 25 m/s.

appear. Notice that the blue line in the left subplot corresponds to a stationary wind speed of 12.8 m/s, which is utilized since the gain of the system becomes zero for a wind speed equal to 12 m/s, when operating along the nominal operating trajectory. This is obvious from Figure C.4. According to Figure C.7 each controller gives rise to an overshoot at the higher wind speed of its operating range, where it is further verified that the two controllers behave equally, as dictated by the design. Furthermore, it becomes obvious that slow transient responses are provided at lower wind speeds.

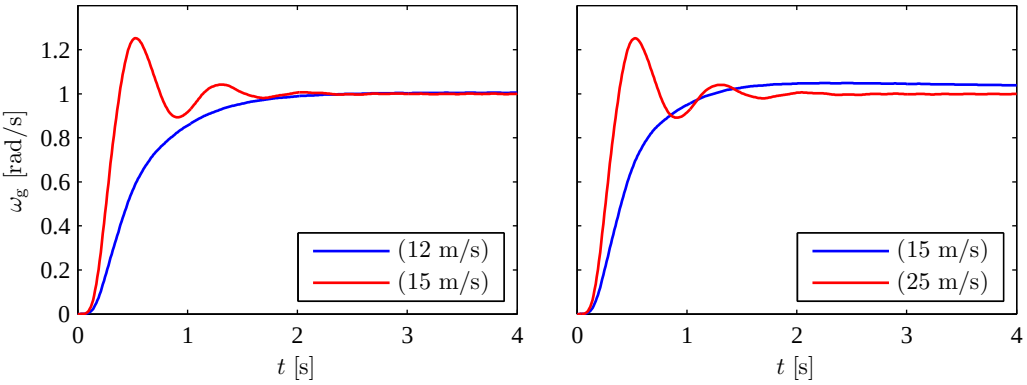

Figure C.7: *Step responses of the speed controllers plotted in the extremes of the operating area.*

So far the two speed controllers have been considered separately. However, at this point the conditions for making transitions between the two controllers are revealed; hereby, finalizing the gain scheduling approach. As the wind speed is considered unknown, the pitch angle is used as an indicator of the current wind speed. This approach is justified by the integral action in the PI controller, as this ensures asymptotic convergence towards the desired operating point for a given wind speed [Hammerum, 2006, p. 30]. Scheduling between the two speed controllers will then happen according to the conditions defined in Table C.2, using the method presented in Section C.4. A hysteresis is introduced through ϵ to avoid oscillations between the two speed controllers.

Evaluation of Speed Controller

Figure C.8 shows how the speed controller performs when keeping the generator torque constant. By doing so, the output power is proportional to the generator speed according to Eq. (3.28) on

Switch	Switching condition
$1 \rightarrow 2$	$\beta(t) \geq \beta_{12} + \epsilon$
$1 \leftarrow 2$	$\beta(t) \leq \beta_{12} - \epsilon$

Table C.2: *Switching conditions, where* $\beta_{12} = 7.98°$ *and* $\epsilon = 0.5°$.

Page 20. This means that the output power depends directly upon the correctness of the model of the power system and of the performance of the speed controller. To circumvent this dependency, a power controller is introduced in the next subsection in order to improve the tracking of the power reference based on a measurement of the power.

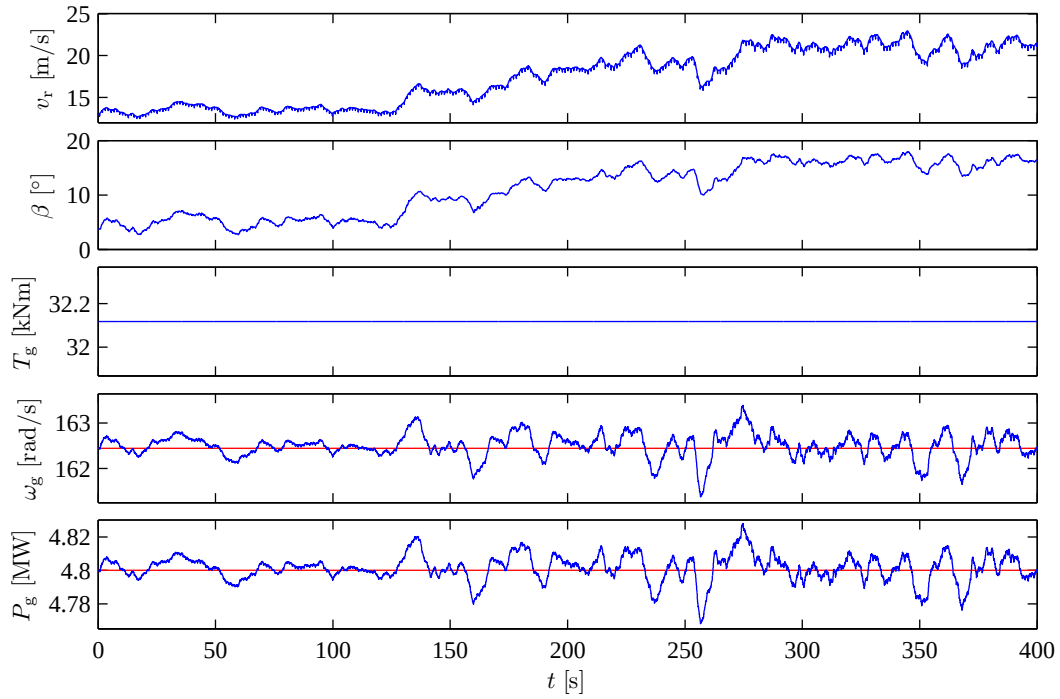

Figure C.8: *Simulation of the speed controller operating above the rated wind speed. Speed Controller* 1 *is active at time* $0 \text{ s} \leq t < 70 \text{ s}$*, while Speed Controller* 2 *operates the wind turbine the rest of the time. Note that the red lines are references.*

Power Controller

The power controller is implemented in order to cancel possible steady-state errors on the output power. This suggests using slow integral control for the power controller, as this will eventually cancel steady-state errors on the output power without interfering with the speed controller. However, it may be beneficial to make the power controller faster to improve accuracy in the tracking of the rated power. To follow this approach the power controller is realized as a PI controller on the form:

$$D_{\text{p}}(s) = K_{\text{pp}} \left(1 + \frac{1}{T_{\text{ip}} \cdot s}\right) \qquad [\text{Nm/W}] \tag{C.10}$$

where:

$D_{\text{p}}(s)$ is the PI controller ensuring that the generated power is close to the rated power [Nm/W]
K_{pp} is the proportional gain of $D_{\text{p}}(s)$ [Nm/W]
T_{ip} is the reset rate of $D_{\text{p}}(s)$ [s]

Applying the measured output power directly is an issue since the measurement is very noisy, as depicted by Section 3.10. This means that measurement noise has to be accounted for in the

design and yields that the proportional gain has to be sufficiently small. The proportional gain is chosen using a trial and error approach while the reset rate is selected large enough to avoid overshoot on the step response. The resulting parameters are shown in Table C.3.

K_{pp}	T_{ip}
$447 \cdot 10^{-6}$ Nm/W	0.031 s

Table C.3: *Parameters for the power controller.*

Evaluation of Power Controller

By adding the power controller to the controller structure, the reference controller operating in the full load region behaves as shown in Figure C.9.

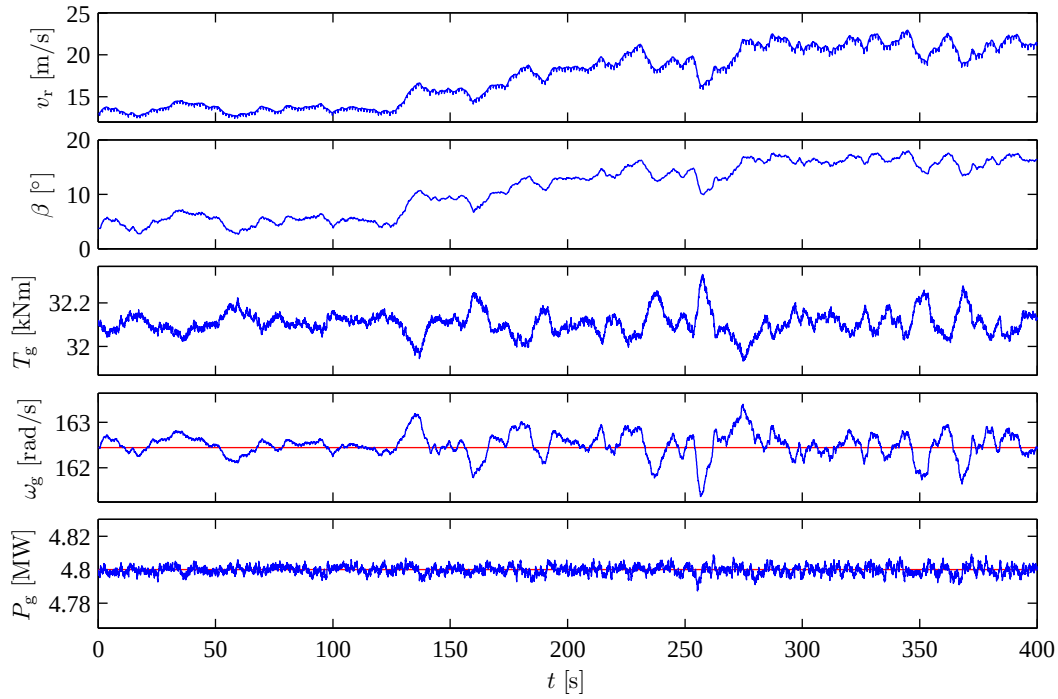

Figure C.9: *Simulation of the cooperative power controller and speed controller operating above the rated wind speed.*

When comparing Figure C.9 to Figure C.8 it is obvious that introducing the power controller results in improved tracking of the power reference. Notice that the differences obtained in the pitch angle and generator speed are neglectable. This states that the power controller improves tracking of the power reference without interfering with the speed controller.

The performance measures evaluating drive train stress and power fluctuations of the two configurations are shown in Table C.4. The results reveal that drive train stress is not increased much by introducing the power controller.

Active controllers	$\int_0^t \dot{\theta}_\Delta^2(\tau)d\tau$	$\int_0^t (P_{g,N} - P_g(\tau))^2 d\tau$
Speed Controller	3.57 nrad^2/s	25.8 GW^{2}s
Speed Controller and Power Controller	3.60 nrad^2/s	2.55 GW^{2}s

Table C.4: *Performance in terms of drive train stress and power fluctuations evaluated during the simulations shown in* Figure C.8 *and* Figure C.9.

At this stage both controllers for operating in partial load and full load have been designed. The next section presents the design of a filter which can be implemented in order to minimize the drive train stress.

C.3 Drive Train Stress Damper

Active drive train damping solutions are deployed in large horizontal-axis wind turbines to mitigate fatigue damage due to drive train oscillations. The idea is to add a component to the generator torque to compensate for the oscillations in the drive train. This signal should have a frequency equal to the eigenfrequency of the drive train, which can be found by filtering the measurement of the generator speed. When the output from the filter is added to the generator torque, the phase of the filter must be zero at the resonant frequency to achieve the desired damping effect.

The drive train damper is implemented to add a compensating torque as shown in Figure C.10.

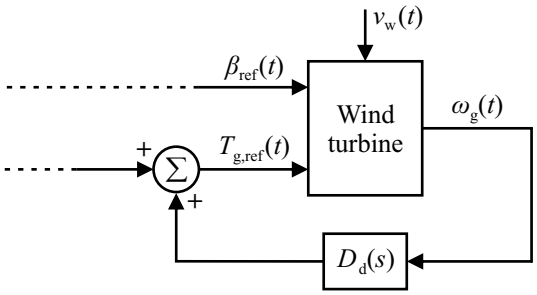

Figure C.10: *Illustration of how the drive train stress damper can be implemented. The dashed lines indicates the control signals coming from the reference controller.*

The following filter structure for the drive train damper is proposed and can be applied to dampen the eigenfrequency of the drive train [Dixit and Suryanarayanan, 2005, p. 1297]:

$$D_{\mathrm{d}}(s) = K_{\mathrm{d}} \frac{2\zeta_{\mathrm{d}}\omega_{\mathrm{nd}} s(1+\tau_{\mathrm{d}} s)}{s^2 + 2\zeta_{\mathrm{d}}\omega_{\mathrm{nd}} s + \omega_{\mathrm{nd}}^2} \quad [\mathrm{Nm/(rad/s)}] \tag{C.11}$$

where:

$D_{\mathrm{d}}(s)$	is the band-pass filter [Nm/(rad/s)]
K_{d}	is the gain of the filter [Nm/(rad/s)]
ω_{nd}	is the undamped eigenfrequency of the filter [rad/s]
τ_{d}	is the time constant which can be used for compensate for time lags in the system [s]
ζ_{d}	is the damping ratio [·]

The time constant τ_{d} introduces a zero in the filter, and can be used to compensate for time lags in the system. Therefore, τ_{d} is selected to equal the time delay of the converter system, $t_{\mathrm{g,d}}$.

The spread of the peak in the amplitude of the frequency response is determined by the damping ratio ζ_{d}, and can be chosen small to give a narrow peak if the eigenfrequency is known precisely. A damping ratio of 0.25 gives a bode plot as shown in Figure C.11.

To determine the gain of the filter, K_{d}, a root locus is plotted for the transfer function from $T_{\mathrm{g,ref}}(s)$ to $\omega_{\mathrm{g}}(s)$ with the filter coupled in a positive feedback loop. The root locus plot is shown in Figure C.12. It is apparent from the figure that if the filter gain becomes too large the system becomes unstable due to the non-minimum phase behavior, introduced by the Padé approximation that resembles the communication delay of the actuator.

Due to the higher loads at higher wind speeds, it is favorable if the filter gain depends on the point of operation. A simple way of fulfilling this property is to apply different gains in the partial and full load configurations of the reference controller; these are 500 Nm/(rad/s) at partial load operation and 2,500 Nm/(rad/s) at full load operation.

By enabling the drive train stress damper in the simulations shown in Figure C.2 on Page 151 and Figure C.9 the drive train stress, evaluated as $\int_0^t \theta_\Delta^2(\tau)d\tau$, is reduced by 50% and 11%, respectively. Hereby, the drive train stress damper is successful in both regions. However, it increases power

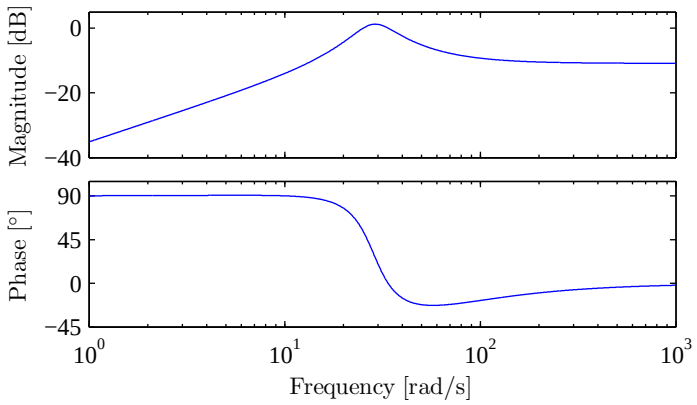

Figure C.11: *Bode plot of the band-pass filter.*

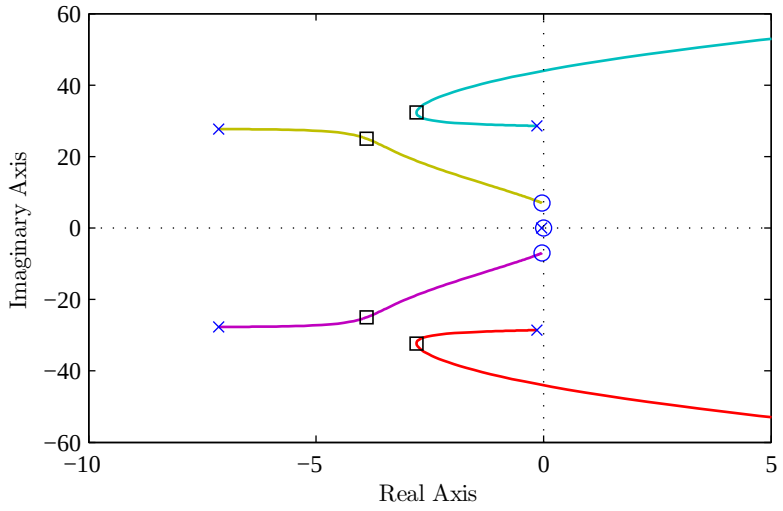

Figure C.12: *Root locus plot of the designed band pass filter and the transfer function from* $T_{\mathrm{g,ref}}(s)$ *to* $\omega_{\mathrm{g}}(s)$*. The poles are marked with crosses and the zeros are marked with circles. The squares represent the location of the closed loop poles when applying the gain chosen for the full load configuration.*

fluctuation in full load operation by working against the power controller to some extent, although it is still beneficial to use the drive train stress damper and power controller in terms of drive train stress and power fluctuations, compared to maintaining the rated generator torque.

The next section addresses the bumpless transfer, which must ensure that no bumps exist on the control signal in the switch between two different controllers.

C.4 Bumpless Transfer

The purpose of this section is to explain how the bumpless transfer mechanism is designed; i.e. how and when to activate the switch illustrated in Figure 2.4 on Page 8. The considered transition is the one that brings the control system from partial load operation to full load operation, and vice versa.

When the control system switches from partial load to full load operation it is important that this transition is not apparent on the control signals; being the generator torque and pitch angle. This is known as bumpless transfer and is important because two controllers may not agree upon the magnitude of the control signal at the time that the transition happens. If a switch between two controllers is undertaken without bumpless transfer, a bump in the control signal may trigger

oscillations between the two controllers, making the system unstable.

The transition from partial to full load operation must happen as the wind speed becomes sufficiently large. For stationary wind speeds this happens at 12.29 m/s, when assuming a single aerodynamic model and absence of tower shadow and wind shear effects. However, it is not convenient to apply the wind speed as the switching condition, since the large inertia of the rotor causes the generator speed and output power to follow significantly later than a rise in the wind speed. Besides, the wind speed is poorly known. Therefore, it is more appropriate to utilize the generator speed as switching condition.

The switching conditions appear in Table C.5. Notice that ϵ is a small number that introduces hysteresis to ensure a minimum time between each transition.

Switch	**Switching conditions**
partial $\rightarrow$ full	$\omega_{\mathrm{g}}(t) \geq \omega_{\mathrm{g,N}}$
full $\rightarrow$ partial	$(\beta(t) \leq \beta_{\mathrm{opt}})$ & $(\omega_{\mathrm{g}}(t) \leq \omega_{\mathrm{g,N}} - \epsilon)$

Table C.5: *Switching conditions where* $\omega_{\mathrm{g,N}} = 162.45$ rad/s, $\beta_{\mathrm{opt}} = 0°$, *and* $\epsilon = 0.2$ rad/s.

Due to the switching condition on $\beta(t)$, and because the output of the speed controller is saturated not to move below 0°, the transition already fulfills bumpless transfer for this control signal. For the generator torque signal a bumpless transfer is assured by adjusting an integral state in such a way that the generator torque will not change abruptly. The compensation torque is calculated using Eq. (C.12), and applies for the transition from Controller 1 to Controller 2; a similar equation applies for the reverse transition.

$$\begin{aligned} T_{\mathrm{g},1}(k) + T_{\mathrm{g,comp}}(k-1) &= T_{\mathrm{g},2}(k) + T_{\mathrm{g,comp}}(k) \\ T_{\mathrm{g,comp}}(k) &= T_{\mathrm{g},1}(k) - T_{\mathrm{g},2}(k) + T_{\mathrm{g,comp}}(k-1) \quad \text{[Nm]} \end{aligned} \tag{C.12}$$

where:

$T_{\mathrm{g},1}(k)$ and $T_{\mathrm{g},2}(k)$ are the torque output from Controller 1 and 2 respectively [Nm]
$T_{\mathrm{g,comp}}(k)$ is the compensation torque which ensures a bumpless transfer [Nm]

The compensation torque is not important when operating above the rated wind speed, because the power controller has integral action. When operating below rated wind speed the compensation torque is discharged to zero, as it otherwise would result in the optimal tip-speed ratio not being followed.